INTERNATIONAL JOURNAL OF HYDROGEN ENERGY 46 (2021) 32695–32709

Available online at www.sciencedirect.com

ScienceDirect

journal homepage: www.elsevier.com/locate/he

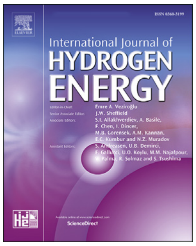

The role of hydrogen in the edge dislocation mobility and grain boundary-dislocation interaction in α-Fe

Mehmet Fazil Kapci [a], *J. Christian Schön* [b], *Burak Bal* [a,*]

[a] *Department of Mechanical Engineering, Abdullah Gül University, 38080, Kayseri, Turkey*
[b] *Max Planck Institute for Solid State Research, Heisenbergstr. 1, 70569, Stuttgart, Germany*

HIGHLIGHTS

- Atomistic origin of hydrogen embrittlement is studied by molecular dynamics simulations.
- Hydrogen decreases edge dislocations mobility by influencing the kink-pair formation.
- Pinning effect of hydrogen causes hardening during pre-existing dislocation activity.
- Hydrogen decreases the critical stress for dislocations emission and facilitates softening.
- Hydrogen inhibits the slip transmission across grain boundary.

ARTICLE INFO

Article history:
Received 28 April 2021
Received in revised form
6 July 2021
Accepted 12 July 2021
Available online 31 July 2021

Keywords:
Hydrogen embrittlement
Molecular dynamics
Dislocation
Fracture

ABSTRACT

The atomistic mechanisms of dislocation mobility depending on the presence of hydrogen were investigated for two edge dislocation systems that are active in the plasticity of α-Fe, specifically ½<111>{110} and ½<111>{112}. In particular, the glide of the dislocation pile-ups through a single crystal, as well as transmission of the pile-ups across the grain boundary were evaluated in bcc iron crystals that contain hydrogen concentrations in different amounts. Additionally, the uniaxial tensile response under a constant strain rate was analyzed for the aforementioned structures. The results reveal that the presence of hydrogen decreases the velocity of the dislocations – in contrast to the commonly invoked HELP (Hydrogen-enhanced localized plasticity) mechanism -, although some localization was observed near the grain boundary where dislocations were pinned by elastic stress fields. In the presence of pre-exisiting dislocations, hydrogen-induced hardening was observed as a consequence of the restriction of the dislocation mobility under uniaxial tension. Furthermore, it was observed that hydrogen accumulation in the grain boundary suppresses the formation of new grains that leads to a hardening response in the stress-strain behaviour which can initiate brittle fracture points.

---

* *Corresponding author.*
E-mail address: burak.bal@agu.edu.tr (B. Bal).

https://doi.org/10.1016/j.ijhydene.2021.07.061

Introduction

The embrittlement effect of hydrogen in metals was firstly discovered in 1875 by Johnson when studying changes of the macroscopic mechanical properties of a piece of iron that had been immersed in hydrochloric and sulphuric acids [1]. The presence of H in the metal facilitates the transition from ductile to cleavage type in the macroscopic fracture process when applying external stresses. This degradation of the mechanical properties causes failures of the material in a great number of engineering applications such as storage tanks, oil gas pipelines, structural components relying on high-strength steels and alloys, etc. [2–6]. Reduction in the yield and tensile stresses by the effect of hydrogen was observed in many previous studies including the deformation at slow, quasistatic, and high strain rates [7–10]. Additionally, hydrogen was reported to decrease ductility, facilitate crack propagation and, decrease fracture toughness that can result in brittle transgranular or intergranular crack formation in the microstructure [11–13]. Nonetheless, degradation of these properties by the presence of hydrogen depends upon several factors, such as hydrogen content exposure, mechanical state, and microstructural properties of the material [14,15]. There exist many models and theories which try to explain the embrittlement mechanism of metals due to hydrogen [16–18], and it is imperative to understand the underlying complexities involved. Discovering the fundamental mechanisms of hydrogen embrittlement (HE) requires information about the source of hydrogen - usually via chemical absorbtion of hydrogen atoms from the metal surface, or due to a release of hydrogen from chemical reactions inside the material -, and also about the diffusion of hydrogen through the lattice and its interaction with microstructural trap sites such as dislocations and grain boundaries [19,20].

Although the exact mechanism of hydrogen embrittlement remains unclear and various factors can contribute to the ultimate response, there are three generally accepted main mechanisms: hydrogen enhanced decohesion, hydride formation, and hydrogen enhanced localized plasticity. The hydrogen enhanced decohesion (HEDE) mechanism suggests that the diffused hydrogen decreases the cohesive energy between the metal atoms in the lattice and weakens the bonding across the atoms at the crack tip, which leads to the sequential separation of the layers and enhancement of the crack propagation under tensile stress [21,22]. Additionally, many experimental and theoretical studies support a mechanism according to which the accumulated hydrogen along grain boundaries can lead to an increased likelihood of fracture by intergranular crack formation [23–26]. Finally, the hydride formation mechanism suggests that regions with high hydrostatic stress, such as those ahead of the crack tip, can accumulate a large amount of hydrogen. This leads to the formation of brittle hydride phases, in particular, in the presence of hydride forming alloying elements V, Zr, Nb, Ta, Ti etc., which results in the propagation of the crack through the brittle phase [16,27]. For systems that do not form hydrides, hydrogen enhanced localized plasticity (HELP) is another frequently invoked mechanism involving the movement of dislocations: Based on the examination of fracture surfaces, Beachem [28] proposed the enhancement of the dislocation mobility in the presence of mobile hydrogen, which leads to an increased plasticity localized at the crack tips and thus causes brittle cleavage already for low applied stresses. Subsequently, this theory was supported by theoretical studies of Birnbaum and Sofronis [29]. Beside noting the effect of hydrogen on the velocity of the dislocations, they also claimed that hydrogen can shield the elastic stresses facing the dislocation due to elastic obstacles such as other dislocations, thereby contributing to the enhanced localized plasticity.

Dislocation behavior in materials containing hydrogen has also been investigated by in-situ TEM and HVEM tools [30,31]. It was proposed that the presence of hydrogen increases the dislocation velocities, and that stress shielding can reduce the distances among dislocations, resulting in pile ups, and between dislocations and defects that can serve as pinning points of the dislocations such as grain boundaries and solutes. Again, it has been observed that in the presence of hydrogen, the cracks can propagate already under low stresses, due to the localized plastic behavior ahead of the crack tip which is associated with an enhanced dislocation velocity and higher emission rate of new dislocations from the crack tip. However, due to the small size of the hydrogen atoms and the difficulty to keep track of the dislocations in-situ, it is difficult to establish an explicit and statistically valid correlation between the dislocation mobility and the hydrogen concentration only from experimental data. Therefore, atomistic modelling of the hydrogen-defect containing structures is required to elucidate the underlying mechanisms.

There exist many studies investigating the role of hydrogen on the embrittlement mechanism via molecular dynamics simulations. Several investigations of the crack propagation in α-iron and nickel crystals reveal that hydrogen accumulated around the crack tip can inhibit the dislocation emission that leads to a ductile to brittle failure transition ahead of the crack tip [32–36]. Furthermore, hydrogen segregation along the grain boundaries and intergranular cleavage leading to a decrease of the cohesive energy has also been observed for various grain boundary orientations and grain sizes [37,38]. An important phenomenon to be understood is the role of hydrogen in the dislocation mobility and in the effective interaction of the dislocation with other defects. Several atomistic studies support the claim that hydrogen enhances the dislocation mobility and leads to a shielding of the stresses acting on dislocations [35,39]. On the other hand, in a study of the effect of hydrogen on α-iron ½<111>{110} edge dislocation pile ups, Song and Curtin [40] suggested that, unlike the previous TEM observations that supported the HELP mechanism, hydrogen does not increase the velocity of the dislocation but rather acts as a drag on the dislocations and thus decreases the velocity, and, in addition, no remarkable shielding can be observed when the dislocations encounter an elastic obstacle. Moreover, for the same dislocation orientation, Zhu et al. [41] claimed that vacancies containing hydrogen have a pinning effect on the dislocation, and that the strength of the pinning increases with the concentration of hydrogen trapped in the vacancy. Katzarov et al. [42] investigated the mobility of screw dislocations in α-iron using the kinetic Monte Carlo approach; they suggested that although for low hydrogen concentrations and applied stresses the velocity of dislocations increases, for higher hydrogen concentrations the dislocation velocity is lower than the one without hydrogen due to a dragging effect of the hydrogen atoms.

In the current study, the effect of hydrogen on the mobility of dislocations was investigated for two slip systems (½<111>{110} and ½<111>{112} edge dislocations) of α-iron by using molecular dynamics. Furthermore, the interaction of the ½<111>{112} dislocations with the Σ3<110>(112) symmetric tilt grain boundary was studied for different hydrogen concentrations. Lastly, single crystal and bicrystal structures with dislocations exposed to tensile loadings were studied with the goal to understand the effect of hydrogen on the reaction of the system to applied tensile stresses.

Simulation models

Molecular dynamics (MD) simulations were performed using LAMMPS (Large-scale Atomic/Molecular Massively Parallel Simulator) [43] on α-Fe crystals. Under pure shear loading, the mobility of ½<111>{110} and ½<111>{112} edge dislocations was examined for different hydrogen concentrations. The two orientations were chosen, because the <111> direction and the {110} and {112} planes are the most dominant slip systems in α-Fe, and in other bcc crystals as well [44,45]. Additionally, transmission across of the ½<111>{112} dislocations through the grain boundary in the presence of hydrogen was investigated by using a symmetric tilt-high angle grain boundary Σ3<110>(112) that has the lowest energy among the various grain boundary types of interest in this system [46]. Finally, uniaxial tensile loadings were performed for the three aforementioned configurations, in order to understand the effect of the hydrogen-defect interaction on the overall mechanical response.

The interatomic interactions among Fe and H atoms were described by using an EAM (embedded atom method) potential developed by Ramasubramaniam et al. [47] where the hydrogen binding energies at the vacancy, free surface, and edge-screw dislocation cores were tested and compared with other ab-initio calculations. Additionally, this potential was used in previous MD studies relying on the accurate prediction of H-defect interactions [48–50]. The total energy is given by Ref. [51].

$$E = \sum_{i} F_{i}\left(\rho_{i}\left(\overrightarrow{r}_{i}\right)\right) + \frac{1}{2} \sum_{j,i} \varnothing\left(r_{ij}\right). \tag{1}$$

F_i is the embedding energy as a function of ρ_i which denotes the electron density at position $\overrightarrow{r}_i$ and $\varnothing$ is the electrostatic pair potential between atoms i and j that only depends on their separation distance r_{ij}. Configurations were displayed by OVITO software [52], and dislocation analyses were performed using the dislocation extraction algorithm DXA [53]. Atomic stress calculations were conducted via the virial stress theorem [54];

$$\sigma_{i} = \frac{1}{V}\left(- m_{i}\frac{d\boldsymbol{u}_{i}}{dt} \otimes \frac{d\boldsymbol{u}_{i}}{dt} + \frac{1}{2} \sum_{j(\neq i)} \boldsymbol{r}_{ij}\Big| \otimes \boldsymbol{f}_{ij}\right) \tag{2}$$

where V is the volume that was calculated by the Voronoi tessellation method, m_i and u_i are the mass of the particle i and the displacement relative to a reference position, respectively, $\boldsymbol{r}_{ij}$ is the vector between particles i and j, and $\boldsymbol{f}_{ij}$ denotes the interatomic force between the two particles.

Dislocation velocity in a single crystal

Single crystal simulations were conducted by using two different bcc iron crystallographic orientation sets of simulation cells with dimensions of 500 Å × 250 Å × 30 Å for the x, y and z directions, respectively. Each simulation cell contains five periodically arranged and equally spaced dislocations that were located 100 Å apart along a line in the x direction in the center of the cell; the glide planes are oriented along y and the Burger's vectors were oriented along the x direction (see Fig. 1). Periodic boundary conditions were used along the x and z directions, and a shrink-wrapped boundary along the y direction was utilized for each simulation cell, i.e., atoms are encompassed by the boundary along the y direction. In order to observe the dislocation velocity under shear stress, a 25 Å region at the bottom ($y = y_{bottom}$) was kept fixed and a 25 Å region at the upper part ($y = y_{top}$) was treated as rigid; in this top region, every atom was exposed to a force parallel to the x direction, such that an average shear stress τ_{xy} of 1 GPa was established. Fig. 1 illustrates the initial configuration used for the first set of simulations.

For the first set, the directions [111] [1–10], and, [−1-12] of α-Fe were aligned along the x, y and z directions, respectively, with five equally spaced (periodic) ½<111>{110} dislocations along the center line parallel to the x direction. For the second set, the [111], [−1-12] and [1–10] directions were oriented along x, y and z directions, respectively, with again five equally spaced ½<111>{112} dislocations along the center line in the x direction with the same simulation cell dimensions and initial boundary conditions. After constructing the initial configurations, hydrogen was introduced to each of the two orientation sets with concentrations of 0.25% H/Fe, 0.5% H/Fe and, 1% H/Fe. Fig. 2 shows the configuration with 0.25% H/Fe concentration for the first set of orientations.

Prior to loading, the energy was minimized for each simulation cell and the system temperature was equilibrated via NVE ensemble simulations for 50 ps by rescaling the temperature of the atoms to 300 K in each step, in order to let the hydrogen atoms diffuse through the system; usually, the H-atoms reside at various interstitial positions in equilibrium. Finally, a constant average force was exerted on the atoms belonging to the upper part of the simulation cells (at $y = y_{top}$) parallel to the x direction, $\overrightarrow{F} = F_{avg}\widehat{x}$, that is computed via the formula

$$F_{avg} = \frac{\tau_{xy} \times (l_x \times l_z)}{n} \tag{3}$$

Here, τ_{xy} is the shear stress exerted on the region that contains the dislocations, l_x and l_z are the length of the supercell along the x and z directions, and n is the total number of atoms in the rigid part at $y = y_{top}$. The loading stage simulation was performed for 50 ps for two crystallographic orientations and all hydrogen concentrations studied.

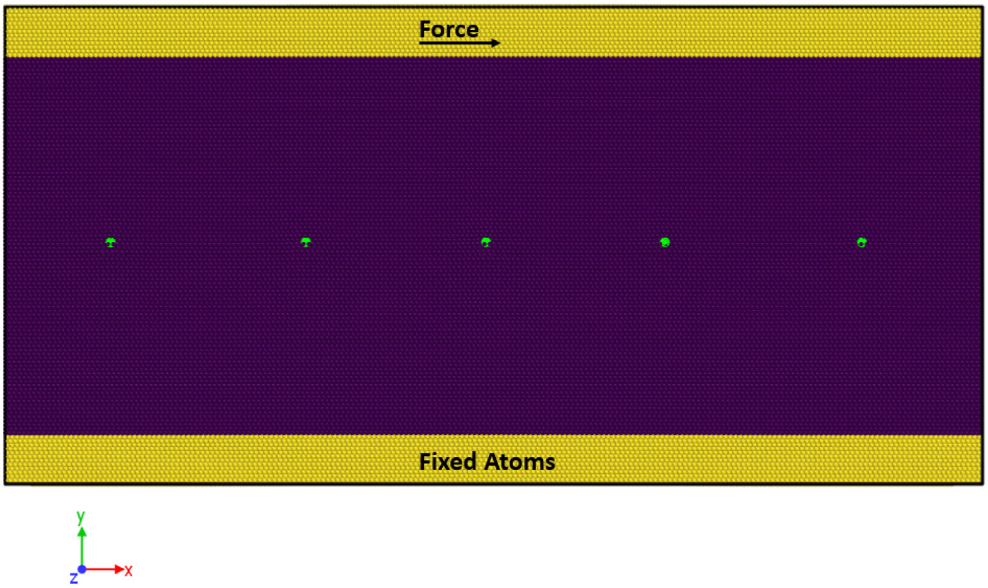

Fig. 1 – Initial configuration for the dislocation velocity simulations in a single crystal with ½<111>{110} dislocations.

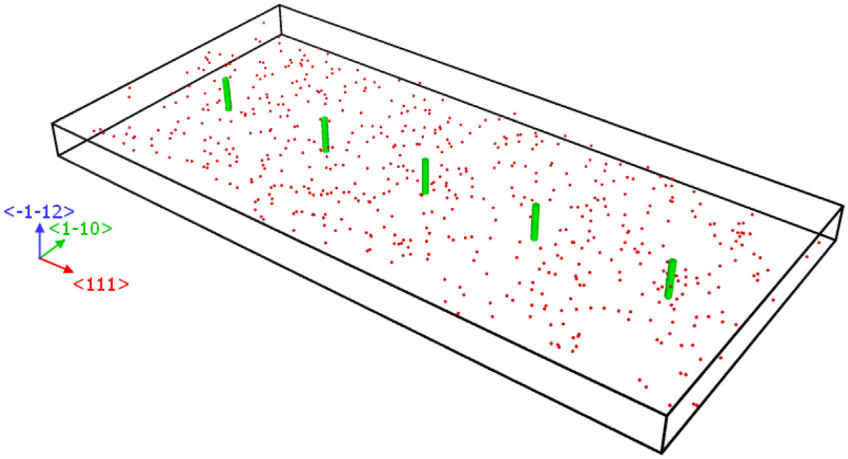

Fig. 2 – Initial configuration of the simulation cell containing five ½<111>{110} dislocations, with 0.25% H/Fe concentration. Recall: the directions [111] [1−10], and, [−1−12] of α-Fe are aligned along the x, y and z directions, resepctively.

Grain boundary-dislocation interaction

In order to evaluate the effect of hydrogen on the transition of the ½<111>{112} dislocations through the $\Sigma3$<110>(112) symmetric tilt grain boundary, a simulation cell of the same size as the one in the single crystal case was generated. The structure consisted of 2 crystals of equal size that were connected via a tilt grain boundary, and which contained a total number of 6 equally spaced dislocations. The normal vectors of the two grain boundary planes were oriented in the x direction, and the grain boundaries were located in the middle and at the border of the periodically repeated simulation cell. The initial configuration is shown in Fig. 3. Regarding the hydrogen concentrations, we employed the same ones as we had for the single crystal simulations (0.25%, 0.5% and 1%), and, similarly, the energy minimization step was followed by a NVE ensemble simulation at 300 K to equilibrate the temperature prior to shear loadings for 50 ps. For the shear loading, the force was again applied to the atoms at the upper part of the cell ($y = y_{top}$); however, a shear stress of 1.5 GPa was applied and the loading stage simulations were performed for 150 ps.

Tensile properties

Simulations of tensile properties were performed for each of the three systems in order to elucidate the mechanical response of the structures containing defects as function of hydrogen content. For the single crystals, not only the aligned sequence of five dislocations (Fig. 1) was used, but also the dislocations that had been randomly distributed through the simulation cell (Fig. 4), and for the bicrystal the same initial configuration (Fig. 3) was used. We first relaxed the hydrogen-free initial configurations at 0 GPa pressure, and afterwards equilibrated the temperature (in the NVE ensemble) and then

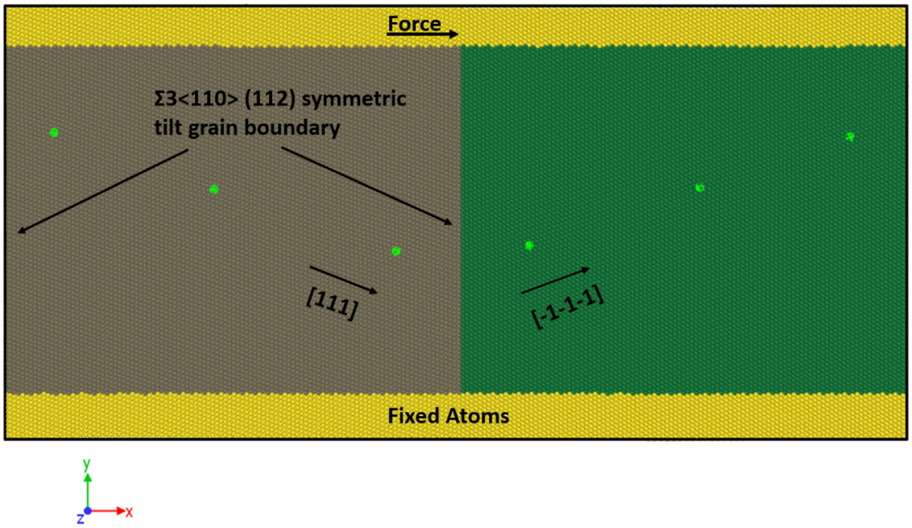

Fig. 3 – Initial configuration for the simulations containing six dislocations and two grain boundaries, one in the center and one at the border of the simulation cell.

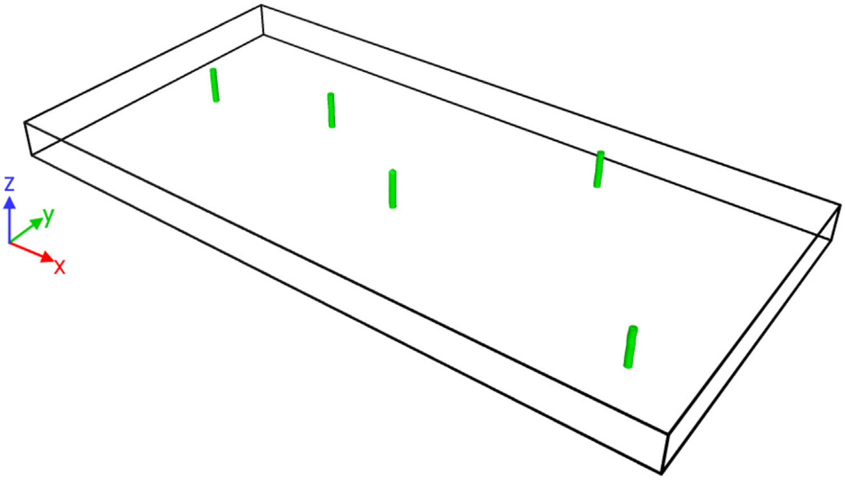

Fig. 4 – Randomly distributed five dislocations through the simulation cell for tensile simulations.

the pressure (in the NPT ensemble) at 300 K and 0 GPa pressure for 50 ps with periodic boundary conditions in all three directions. We also employed periodic boundary conditions along the y direction rather than shrink-wrapping as in the previous simulations; since there are extra half planes of atoms for each dislocation at the upper side of the dislocations, new dislocations were formed and more dislocations were obtained for each simulation set. After this stage, hydrogen atoms were inserted into each structure, again with concentrations of 0.25%, 0.5% and 1%, and the temperature was equilibrated at 300 K. For all subsequent simulations, a uniaxial tensile load was applied parallel to the x direction with the strain rate of 10^{-3} 1/ps (10^{9} 1/s) with periodic boundaries in all directions up to a 50% strain. The simulations were then performed in the NPT ensemble by keeping the pressure at 0 GPa along y and z.

Results

Dislocation velocity in a single crystal

Before evaluating the dislocation mobility under shear load, virial stresses and total energy of the dislocations were investigated after the temperature equilibration. The (local) total energies per atom of the Fe atoms within the 5 Å cut-off around the dislocation cores ($E_{dislocation}$) were calculated for each simulation cell (Fig. 5a). Fig. 5b shows the average normalized energy $\tilde{E}$ of the dislocations with respect to the energy of the reference crystal ($E_{reference}$):

$$\tilde{E} = \frac{E_{dislocation} - E_{reference}}{|E_{reference}|}. \tag{4}$$

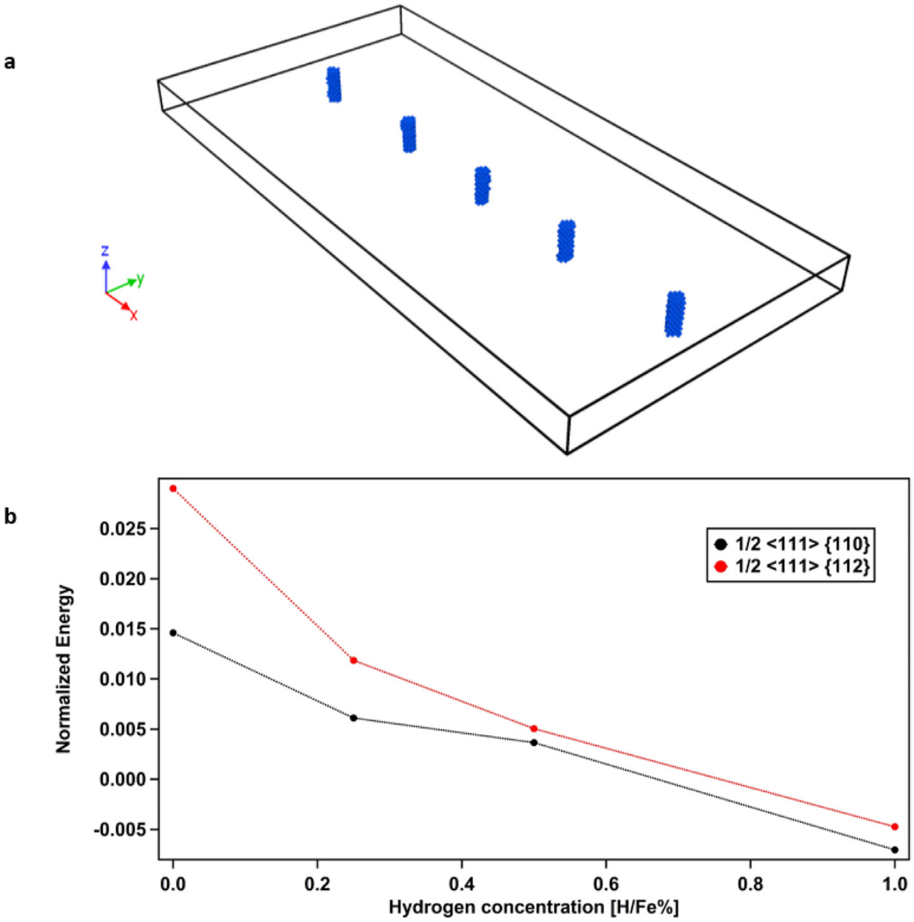

Fig. 5 – a) Fe atoms within the 5 Å cut-off from the dislocation cores in the case with ½<111>{112} dislocations and 0% hydrogen concentration. b) Normalized energy values for two glide planes and four hydrogen concentrations.

For both systems, the local energy of the system with dislocations was larger than the one for the reference system if no hydrogen atoms had been added, i.e., $\tilde{E} > 0$, where the ½<111>{112} dislocations caused a larger energy increase than the ½<111>{110} dislocations. In both systems, it was found that the local energy of the crystal distortion at the dislocation cores was reduced by the hydrogen accumulation for each glide plane, where a larger energy change was observed for the ½<111>{112} dislocations. However, for a hydrogen concentration of 1%, both systems were found to be more stable when compared to the reference state, i.e., $\tilde{E} < 0$.

Furthermore, virial stresses in the x direction were evaluated both for the compressive and tensile region within a 40 Å wide (in the y-direction) band along the x direction above and below the line at $y = 125$ Å, on which the dislocations had been placed (Fig. 6a). It was observed that hydrogen accumulation increases the compressive stress σ_{xx} in the 20 Å wide region above the dislocation core (125 Å < y < 145 Å) in the overall behaviour; here, the 0.25% H concentration shows a larger stress value compared with the 0.5% case, for the ½<111>{112} dislocations (Fig. 6b). A more monotnoic increase in the magnitude of the stress field was observed in the tensile region, 105 Å < y < 125 Å, for both types of dislocations (Fig. 6c), where hydrogen accumulation in the dislocation core reduced the stresses for both glide planes. It should be noted that unlike the potential energy of alpha-Fe, the magnitude of the change in the stress was higher for the ½<111>{110} dislocations.

The average dislocation position in the direction of the Burger's vector as a function of time is shown in Fig. 7a and b, and in Fig. 7c and d, the velocities, respectively, for the ½<111>{110} and ½<111>{112} periodic dislocations. It was observed that the velocity of dislocations decreases with increasing H concentration for both orientation sets, with a strong effect for the 1% H-concentration in the ½<111>{112} dislocation set. Moreover, the point in time when the dislocation started to due to the accumulated shear stress in the initial stages of the shear loading step of the simulations, was delayed by the presence of hydrogen around the dislocation cores. It can be concluded that hydrogen has a pinning effect for both slip systems and that it is more active along the {112} glide plane. In summary, it was found that the presence of hydrogen decreases the velocity of the edge dislocation in α-iron, with the amount depending on the slip system and the dislocation movement regime under consideration. Although the separation distance between the dislocations is stable for both glide planes, the pinning of the ½<111>{112} dislocations is more pronounced for the high hydrogen concentrations.

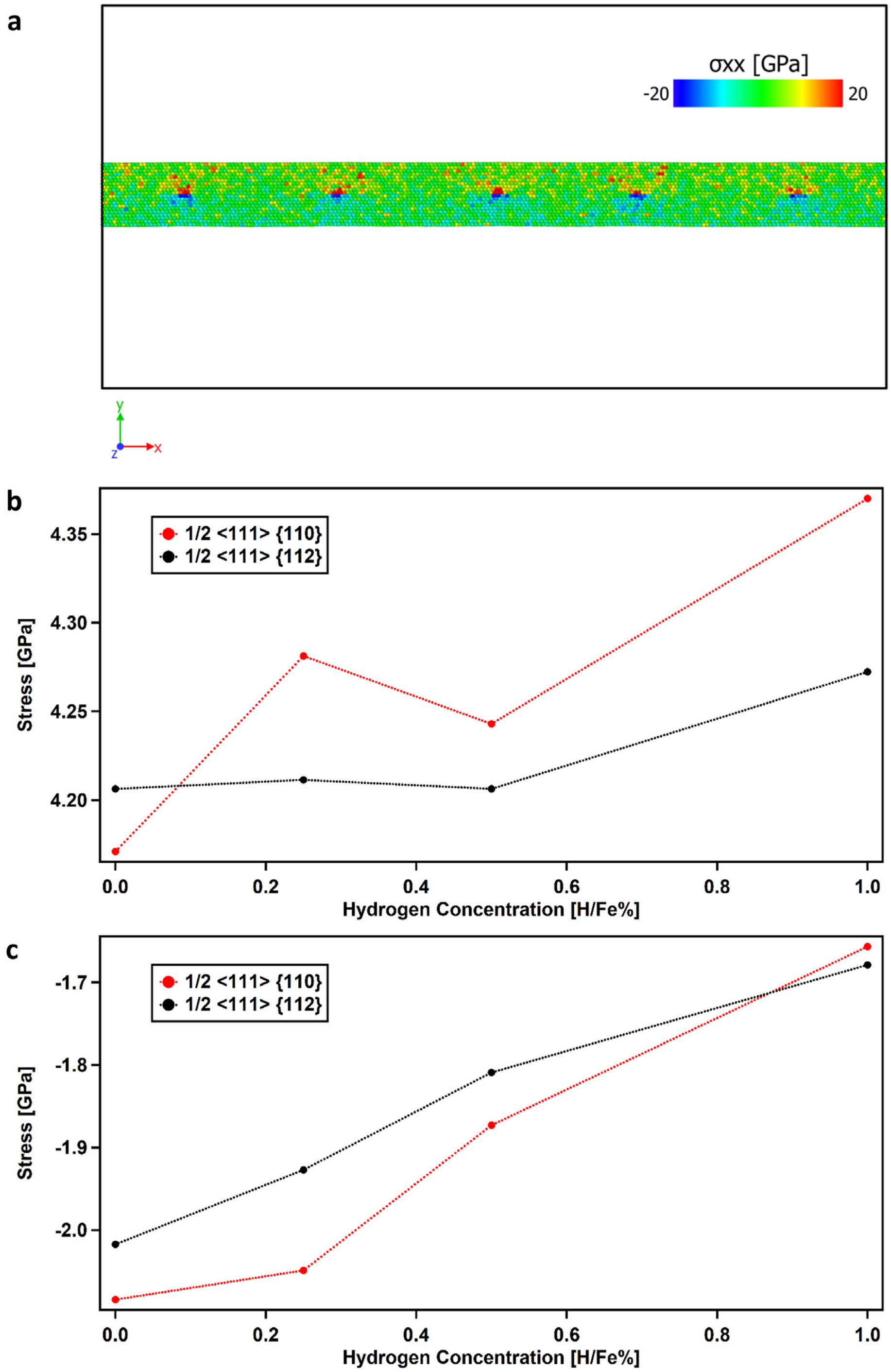

Fig. 6 – a) Tensile and compressive stress (σ_{xx}) representation within the 40 Å wide band around the line of dislocations. Positive stress values corresponds to compressive and negative stress values corresponds to tensile stress, respectively. b) Average stress above the dislocation cores and c) average stress below the dislocation cores for different hydrogen concentrations.

Grain boundary & dislocation interaction

Fig. 8 shows the movement of the ½<111>{112} dislocations in the simulation cell containing two grain boundaries for various hydrogen concentrations. Once a single dislocation closely approaches a grain boundary it gets absorbed by the boundary and requires an additional elastic stress field, e.g., of a subsequent dislocation, to overcome the energy barrier and to continue its movement through the crystal lattice. However, as the hydrogen concentration increases in both the dislocation cores and the grain boundaries, the mobility of the dislocations decreases overall. In the case of no hydrogen (0% H/Fe concentration), after the shear loading, the system stabilizes with two dislocations absorbed in the grain boundaries

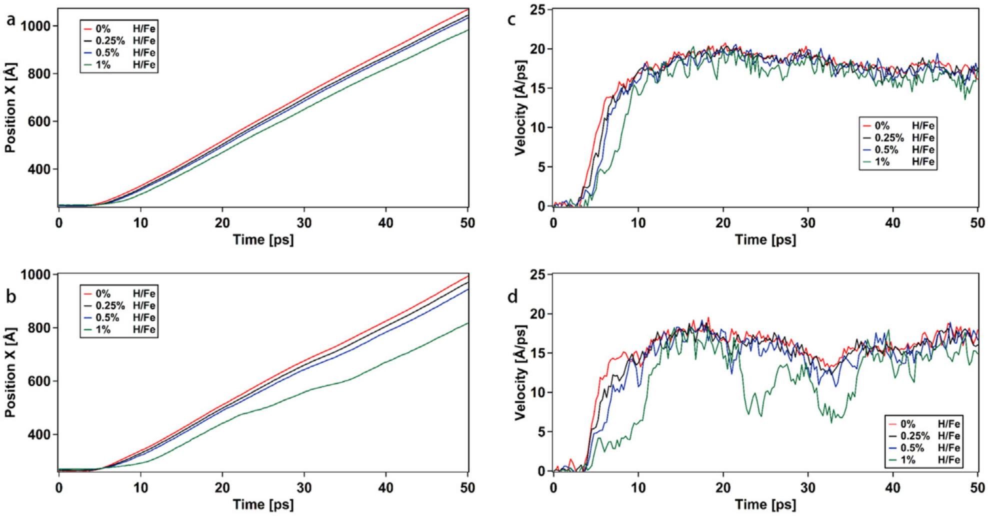

Fig. 7 – Average disloction position x vs time graph for a) ½<111>{110} and b) ½<111>{112} periodic dislocations. Average instantaneous velocities of c) ½<111>{110} and d) ½<111>{112} periodic dislocations.

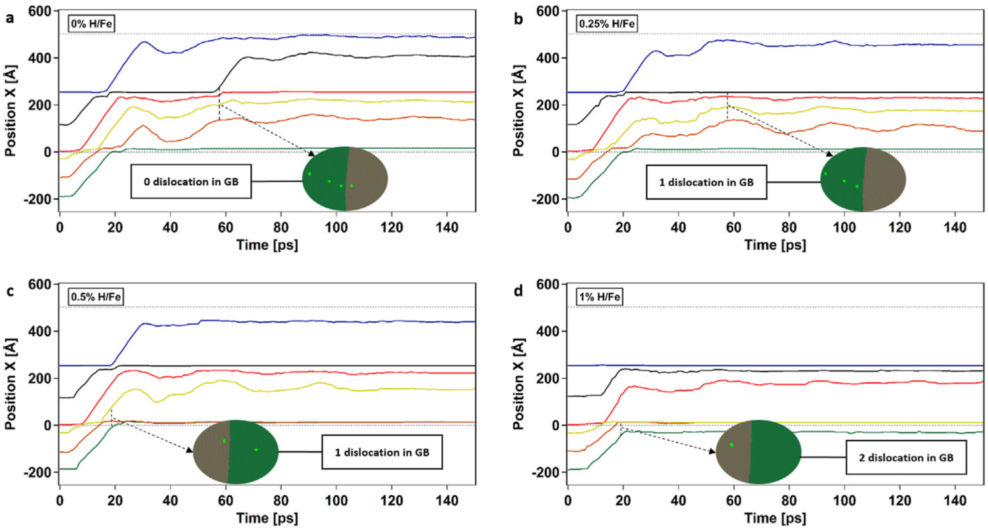

Fig. 8 – X Positions of the single dislocations within the simulation cells containing 2 grain boundaries for a) 0% b) 0.25% c) 0.5% and d) 1% H/Fe concentrations. Grey dots represents the periodic boundaries.

and with a pair of dislocations stuck behind each grain boundary (Fig. 8a). Furthermore, after ca. 50–70 ps, the accumulation of three dislocations behind the absorbed dislocation builds up a strong enough stress field to nucleate the absorbed dislocation into the crystal on the other side of the grain boundary. However, Fig. 8b shows that in the presence of 0.25% H/Fe, the elastic stress fields of the dislocations are insufficient to nucleate, and thus re-activate, the dislocation absorbed in the grain boundary. In fact, at higher hydrogen concentrations, more than one dislocation can be absorbed in the grain boundary as shown in Fig. 8c and d. We conclude from these grain boundary + dislocation simulations that hydrogen can increase local plasticity by shielding the elastic long-range interactions between the edge dislocations and other elastic obstacles. This result is consistent with the shielding effect discussed in the context of the HELP mechanism.

Simulations of tensile properties

Each of the three supercell orientations mentioned above was exposed to a tensile loading with a constant strain rate and periodic boundaries in all three dimensions in order to evaluate mechanical characteristics and the effect of hydrogen on the pre-existing defects. For the structures without grain boundaries, no fracture was observed up to 50% strain. In contrast, in the supercell containing a grain boundary, intergranular cleavage surfaces were obtained after the deformation-induced grain formation by the same Σ3<110>(112) symmetric tilt grain boundaries.

We first discuss the simulations with single crystals. In the simulations that contained ½<111>{110} dislocations from the outset, all simulation cells showed a similar elastic response and yield stresses were decreased gradually by increasing hydrogen concentration. An immediate softening was observed by yielding with the formation of new dislocations; for increasing H/Fe concentration, the softening process starts earlier, and the pre-existing dislocations showed no mobility for all simulation cells. Tensile stress versus strain graphs are shown in Fig. 9.

For the simulations with ½<111>{112} dislocations, each configuration showed the same elastic modulus and a hardening stage was observed after yielding with the mobility of pre-existing dislocations (Fig. 10). Hydrogen was observed to delay and restrict the mobility of the pre-existing dislocations. Also, depending on the hydrogen concentration, dislocations were observed to follow different paths during hardening. In all simulations for the four hydrogen concentrations, the pre-exisiting dislocation mobility was observed along the [−1-11] direction after the yielding that corresponds to the hardening phase. It was also observed that the mobile pre-existing ½<111> dislocations form a junction and nucleate 1<001> dislocations when they encounter each other (Fig. 11). It was found that the pinning effect of hydrogen on the pre-existing dislocations increases the stress by inhibiting the pre-existing dislocation activity.

Turning to the simulations in the presence of grain boundaries, Fig. 12 shows the stress-strain behaviour for simulation cells containing the two grain boundaries and dislocations, for various hydrogen concentrations. Unlike the single crystal simulations, pre-existing dislocation activity starts immediately after the tensile load was applied in the x direction. For each hydrogen concentration, the pre-existing ½<111>{112} dislocations follow the same path and glide in the <111> direction until every dislocation is absorbed in the grain boundary. Our results reveal that the presence of hydrogen restricts the movement of the dislocations in proportion to the hydrogen concentration and eventually increases the stress for the same strain levels. After that, a softening stage begins with the formation of a new Σ3<110>(112) grain boundary along the [111] direction inside the single crystal part. We observed that the presence of hydrogen inhibits the formation of new grain boundaries and thus, eventually, inside the supercell more stress accumulates during the loading. Fig. 13 shows the grain configurations for the simulation cells with four different H-concentrations, at the same strain level (7.5%).

Discussion

During the movement of a dislocation through the crystal lattice, different regimes and mechanisms can play a role depending on the temperature, applied stress, and slip system. At 0 K temperature, an infinitely long dislocation needs to exceed the so-called Peierls stress in order to start the glide along the Burger's vector direction [55,56]. It is known that the Peierls stress for the ½<111>{112} dislocation is significantly higher than the one for the ½<111>{110} dislocation. Owing to the asymmetrical core structure, the {112} glide plane exhibits different critical stresses depending on the loading direction especially for low temperatures [57]. We note that in one regime, the dislocation movement through the crystal lattice is controlled by the phonon drag dynamics [58]. During the movement of the dislocation, a drag force is acting on the dislocation with a drag coefficient $B(T)$ which depends on the temperature, and the velocity of the dislocation can be expressed as [58,59].

$$v = \frac{\tau b}{B(T)}, \tag{5}$$

where τ is the shear stress and b is the magnitude of the Burger's vector. Although several mechanisms contribute to the viscous damping of the dislocation glide, according to this model phonon scattering is the main factor determining the

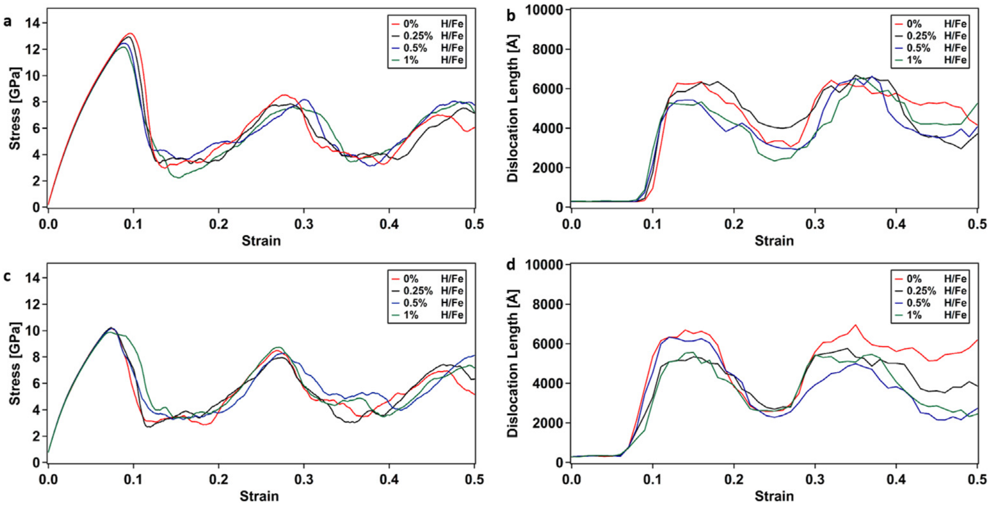

Fig. 9 – Stress and total dislocation length vs strain graphs of the simulation set with ½<111>{110} dislocations, for the single crystal, a,b) for the random initial distribution of the five dislocations, c,d) for the aligned sequence of five dislocations along x axis. Note that the maxima in the dislocation lengths correlate with minima in the stress. Very similar results were observed for the initial distribution with five aligned dislocations: the maximal stress was slightly reduced compared to the random dislocation arrangement, while the strains where the peaks and the minima of the stress and the dislocation lengths occurred were the same.

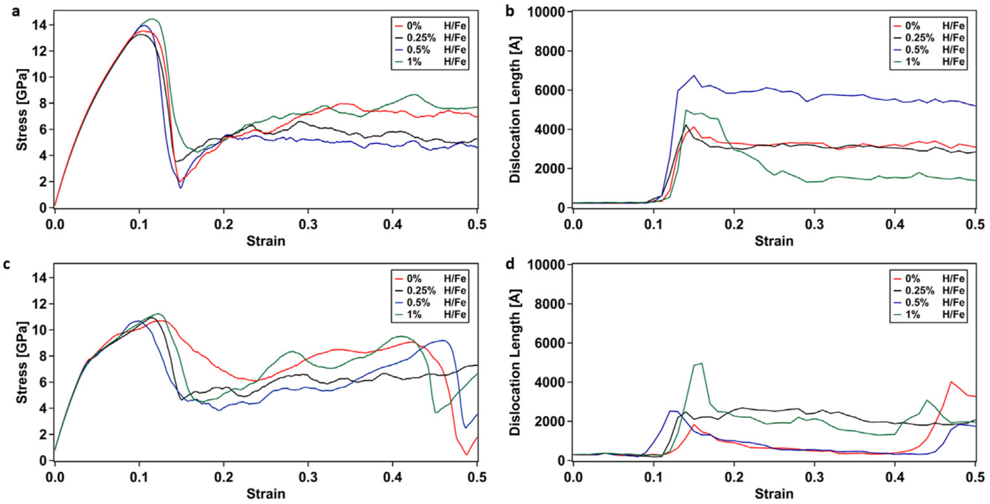

Fig. 10 – Stress and total dislocation length vs strain graphs of the simulation set with ½<111>{112} dislocations, for the single crystal. Again, a,b) the results found for the random initial distribution of the five dislocations, c,d) for the aligned sequence of five dislocations along x axis.

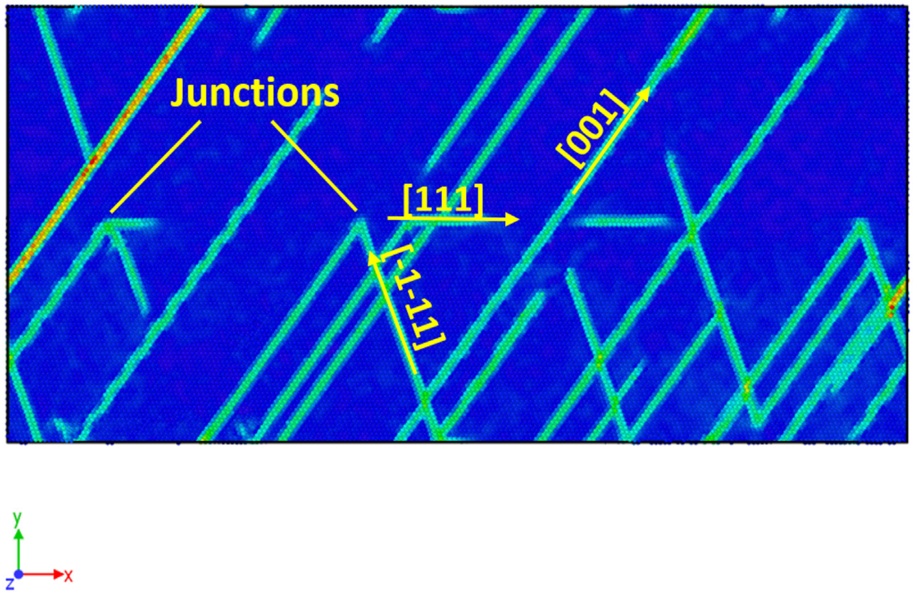

Fig. 11 – Strain paths of pre-existing dislocation in ½<111>{112} dislocation containing supercell after yielding and junction formation, for the single crystal.

drag coefficient [59,60]. However, atomistic and continuum level studies show that although the phonon drag dynamics is capable of modeling the mobility of the {110} glide plane for appropriate stresses and temperatures, more than one regime should be considered [57–59] when evaluating the behavior in the case of a {112} glide plane. It is also possible for dislocations to move at shears below the Peierls stress when the temperature is high enough to generate thermally activated kink pairs. It was observed in a MD study that the motion of the ½<111>{112} dislocation takes place via nucleation of the kink pairs at temperatures below 100 K, while for higher temperatures the drift of kinks is the dominant process [57]. The velocity of the dislocation that moves by the kink pair formation is defined as [61,62].

$$\upsilon_{kp} = \omega_D \frac{bLh}{x_c^2} exp\left[\frac{U_{kp}^{(c)}(\tau)}{kT}\right], \tag{6}$$

where ω_D is Debye frequency, $\frac{1}{x_c}$ is the number of possible kink pair formation sites, L is the length of the dislocation, h is the periodicity in the barrier, and $U_{kp}^{(c)}(\tau)$ is the kink pair activation energy.

In simulations, for both dislocation types, we observed the formation of kinks while the dislocations glide through the

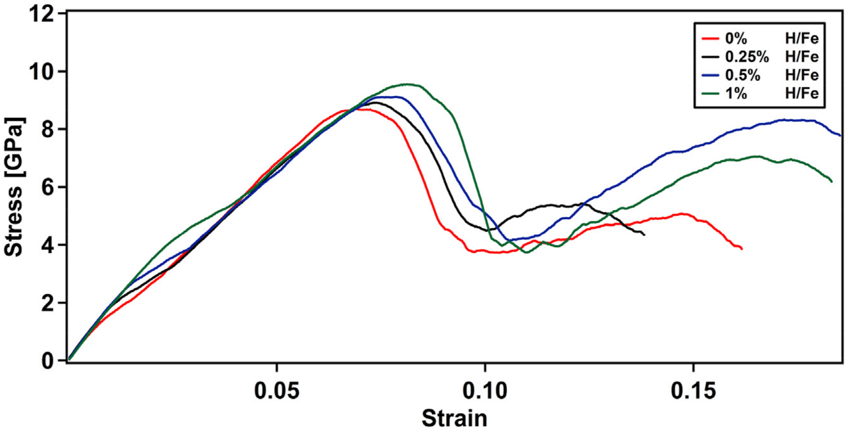

Fig. 12 – **Stress and vs strain graphs of the simulation set with grain boundaries and ½<111>{112} dislocations. Note that the softening earlier than for the case without grain boundaries, c.f. Fig. 9.**

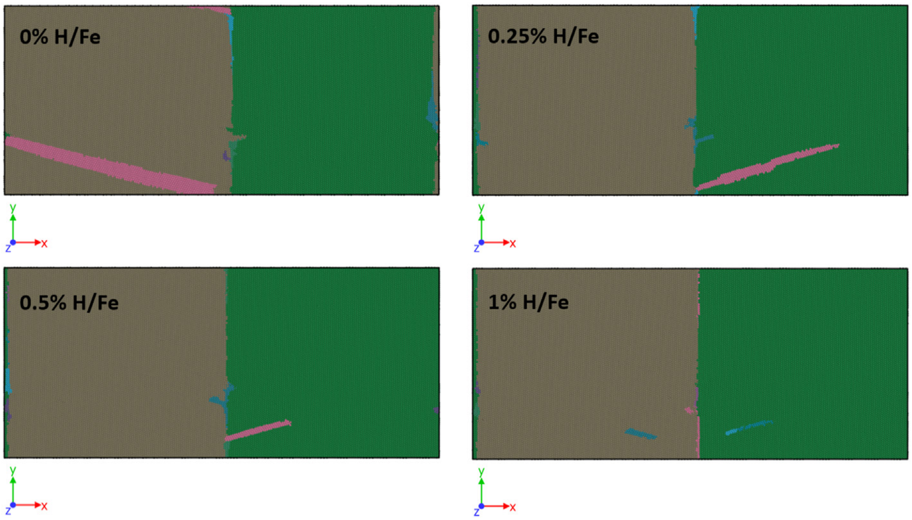

Fig. 13 – **Σ3<110>(112) grain boundary formation at 7.5% strain for %0 H/Fe, 0.25% H/Fe, 0.5% H/Fe, and 1% H/Fe supercells. Each colour represents different grains where the newly formed deformation induced grains have the same Σ3<110>(112) grain boundary. (For interpretation of the references to colour in this figure legend, the reader is referred to the Web version of this article.)**

crystal lattice. However, more rapid kink pair formation and reversion, and also gliding as more straight dislocation lines occurred for the {110} glide plane dislocations. On the other hand, {112} glide plane dislocations showed advancement via the nucleation of kink pairs in comparatively higher numbers and also sustained kink formation for a longer time. These results can also be seen from Fig. 7: unlike the {110} glide plane dislocation, the average position of the {112} dislocation shows a nonlinear advancement due to the trapped kink pairs which become more distinctive as the hydrogen concentration increases. It was observed from the simulations that when a part of a straight dislocation line encounters a hydrogen-rich region, it gets attracted and trapped within that region with a hydrogen rich atmosphere. Based on this observation, hydrogen was proposed to inhibit the nucleation of new kinks by decreasing the number of kink pair formation sites, and also by reducing the activation energy for the kink pair formation process which is dependent to shear stress. Thus, rather than the drag coefficient being changed by a phonon-impurity scattering, the pinning effect by influencing the kink pair nucleation is observed to be the active mechanism for the reduced mobility of dislocations in the hydrogen presence. Moreover, although the hydrogen atoms in the core of the dislocations decrease the elastic stress field of the {110} glide plane by more than for the {112} glide plane, the velocity and the total energy around the dislocations was found to decrease by a larger amount for the {112} glide plane than for the {110} dislocation. As a consequence, when there is hydrogen present in the lattice, the pinning effect was observed to be more pronounced for the {112} glide planes, showing an inhibited mobility of the dislocation movement when the dislocation advancement is based on the kink pair nucleation regime.

In general, restriction of the movement of the pre-existing {112} dislocations was seen to cause more hardening in the behaviour of the uniaxial tensile stress in addition to a delay in the activity of the pre-existing dislocation until the first maximum in the stress has been reached (Fig. 10). Although in the single crystal tensile deformation simulations, the dislocations followed different paths, in the initial stage of the grain boundary simulations each dislocation follows the same path and the hardening occurs with increasing hydrogen concentration (Fig. 12).

Such a hydrogen-induced hardening effect had also been observed in earlier modelling and experimental studies of the pinning role of hydrogen on dislocations movement [63–66]. Unlike the second simulation set with {112} dislocations, structures containing {110} dislocations did not show any dislocation mobility before the emission of new dislocations, since not enough shear stress could accumulate along the <111> direction during tensile loading (Fig. 9). However, the yield stress was sufficiently reduced by the emission of new dislocations when increasing the hydrogen concentration. In earlier studies, it had been found that hydrogen can facilitate dislocation emission by decreasing the critical stress intensity at the crack tip [67,68]. From the uniaxial tensile simulations of the single crystalline structures containing pre-existing dislocations, we conclude that hydrogen presence can suppress plasticity and lead to local brittle regions where restriction of the movement of dislocations leads to hardening. On the other hand, we also found that the presence of hydrogen atoms can enhance plasticity by facilitating the emission of new dislocations if there is no pre-existing dislocation activity and plastic behavior occurs via emission of new dislocations.

Movement of the dislocations in the bicrystals with grain boundaries revealed that hydrogen can lead to localization of the regions with enhanced plasticity near elastic obstacles. It was observed from the simulations that the presence of hydrogen decreases the elastic stress fields around the dislocations (Fig. 6). Furthermore, it was found that in the presence of hydrogen, the transmission of the dislocations across grain boundaries is less likely, due to the reduced elastic field of the sequence of dislocations. Furthermore, a larger energy was required for a dislocation to leave the hydrogen segregated grain boundary. Beside the shielding effect of hydrogen, it was also observed that for a high hydrogen concentration (1% H/Fe), the grain boundary can absorb more than one dislocation, while only one dislocation can be absorbed and emitted at a time for the lower hydrogen concentrations (Fig. 8). In earlier investigations of Ni and Fe symmetric tilt grain boundaries and screw dislocations interactions, it had been observed that when the hydrogen segregates along the grain boundaries, this can increase the energy barrier for the dislocation-GB interactions such as transmission, absorption, and emission [69,70]. Additionally, tensile simulations of the bicrystals reveal that strain-induced grain nucleation was suppressed by the increasing hydrogen concentration. For the same strains, we observed grain formations in various volumes depending on the hydrogen concentration (Fig. 13). Furthermore, in previous molecular dynamics studies on the bcc Fe nanograins, it was found that hydrogen can inhibit the GB-related deformation processes such as grain boundary migration, rotation, sliding, and also dislocation and deformation twin nucleation from the grain boundary due to the grain boundary disorder and reduced mobility of the grain boundaries which eventually suppress the plastic deformation [38,71]. Finally, from the simulations, we can conclude that hydrogen can facilitate the existence of local brittle fracture points around the grain boundary by suppressing the strain-induced grain nucleation.

Conclusions

In summary, we investigated the role of hydrogen on the edge dislocation mobility and also grain boundary-dislocation interactions in alpha-iron. To further evaluate these systems, uniaxial tensile loadings were performed under constant strain rate. The following conclusions can be drawn from the study;

(1) The presence of hydrogen in the crystal lattice decreases the velocity of the edge dislocations and the movement regime is a determining factor regarding the magnitude of the reduced mobility. It was observed that the pinning effect of the hydrogen atoms on the dislocation is more pronounced when the glide occurs via kink pair formation.
(2) When the dislocations encounter an elastic obstacle, hydrogen can shield the elastic stress fields between dislocation pile ups and it can facilitate plasticity localization as suggested in the HELP mechanism. Moreover, the energy required for dislocation transmission across the grain boundary is higher in the presence of hydrogen, which can lead to enhanced plastic behaviour around the grain boundary.
(3) While the pre-existing dislocations are mobile in the single crystal and bicrystal, hardening was observed, suggesting the pinning effect of the hydrogen atoms as the mechanism. Although this can lead to inhibition of plasticity and formation of brittle crack initiation points, it was also shown that hydrogen presence can decrease the required stress for emission of dislocations and actually enhance local plasticity.
(4) Atomic configuration disorder at the grain boundary by segregated hydrogen can contribute to the plasticity localization by increasing defect absorption. However, brittle behaviour was also observed in bicrystals by the reduction of strain-induced grain nucleation capacity under the effect of hydrogen.

Declaration of competing interest

The authors declare that they have no known competing financial interests or personal relationships that could have appeared to influence the work reported in this paper.

Acknowledgments

The work has been performed under the Project HPC-EUROPA3 (INFRAIA-2016-1-730897), with the support of the EC Research Innovation Action under the H2020 Programme. B. Bal also acknowledges the support by the Scientific and

Technological Research Council of Turkey (TÜBİTAK) BIDEB-2219 Postdoctoral Research program under Project no. 1059B192000774.

REFERENCES

[1] Johnson WH. II. On some remarkable changes produced in iron and steel by the action of hydrogen and acids. Proc R Soc Lond 1875;23:168–79. https://doi.org/10.1098/rspl.1874.0024.

[2] Woodtli J, Kieselbach R. Damage due to hydrogen embrittlement and stress corrosion cracking. Eng Fail Anal 2000;7:427–50. https://doi.org/10.1016/S1350-6307(99)00033-3.

[3] Hardie D, Charles EA, Lopez AH. Hydrogen embrittlement of high strength pipeline steels. Corrosion Sci 2006;48:4378–85. https://doi.org/10.1016/j.corsci.2006.02.011.

[4] Oriani RA. Hydrogen embrittlement of steels. Annu Rev Mater Sci 1978;8:327–57. https://doi.org/10.1146/annurev.ms.08.080178.001551.

[5] Koyama M, Akiyama E, Lee YK, Raabe D, Tsuzaki K. Overview of hydrogen embrittlement in high-Mn steels. Int J Hydrogen Energy 2017;42:12706–23. https://doi.org/10.1016/j.ijhydene.2017.02.214.

[6] Song RG, Dietzel W, Zhang BJ, Liu WJ, Tseng MK, Atrens A. Stress corrosion cracking and hydrogen embrittlement of an Al-Zn-Mg-Cu alloy. Acta Mater 2004;52:4727–43. https://doi.org/10.1016/j.actamat.2004.06.023.

[7] Bal B, Koyama M, Gerstein G, Maier HJ, Tsuzaki K. Effect of strain rate on hydrogen embrittlement susceptibility of twinning-induced plasticity steel pre-charged with high-pressure hydrogen gas. Int J Hydrogen Energy 2016;41:15362–72. https://doi.org/10.1016/j.ijhydene.2016.06.259.

[8] Najam H, Koyama M, Bal B, Akiyama E, Tsuzaki K. Strain rate and hydrogen effects on crack growth from a notch in a Fe-high-Mn steel containing 1.1 wt% solute carbon. Int J Hydrogen Energy 2020;45:1125–39. https://doi.org/10.1016/j.ijhydene.2019.10.227.

[9] Zhang Z, Obasis G, Morana R, Preuss M. Hydrogen assisted crack initiation and propagation in a nickel-based superalloy. Acta Mater 2016;113:272–83. https://doi.org/10.1016/j.actamat.2016.05.003.

[10] Rehrl J, Mraczek K, Pichler A, Werner E. Mechanical properties and fracture behavior of hydrogen charged AHSS/UHSS grades at high- and low strain rate tests. Mater Sci Eng, A 2014;590:360–7. https://doi.org/10.1016/j.msea.2013.10.044.

[11] Bal B, Okdem B, Bayram FC, Aydin M. A detailed investigation of the effect of hydrogen on the mechanical response and microstructure of Al 7075 alloy under medium strain rate impact loading. Int J Hydrogen Energy 2020;45:25509–22. https://doi.org/10.1016/j.ijhydene.2020.06.241.

[12] Bal B, Çetin B, Bayram FC, Billur E. Effect of hydrogen on fracture locus of Fe–16Mn–0.6C–2.15Al TWIP steel. Int J Hydrogen Energy 2020. https://doi.org/10.1016/j.ijhydene.2020.09.083.

[13] Laureys A, Depover T, Petrov R, Verbeken K. Characterization of hydrogen induced cracking in TRIP-assisted steels. Int J Hydrogen Energy 2015;40:16901–12. https://doi.org/10.1016/j.ijhydene.2015.06.017. Elsevier Ltd.

[14] Bal B, Sahin I, Uzun A, Canadinc D. A new venue toward predicting the role of hydrogen embrittlement on metallic materials. Metall Mater Trans A Phys Metall Mater Sci 2016;47:5409–22. https://doi.org/10.1007/s11661-016-3708-z.

[15] Barnoush A. Hydrogen embrittlement, revisited by in situ electrochemical nanoindentation. 2007.

[16] Lynch S. Hydrogen embrittlement phenomena and mechanisms. Corrosion Rev 2012;30:105–23. https://doi.org/10.1515/corrrev-2012-0502.

[17] Dwivedi SK, Vishwakarma M. Hydrogen embrittlement in different materials: a review. Int J Hydrogen Energy 2018;43:21603–16. https://doi.org/10.1016/j.ijhydene.2018.09.201.

[18] Martin ML, Dadfarnia M, Nagao A, Wang S, Sofronis P. Enumeration of the hydrogen-enhanced localized plasticity mechanism for hydrogen embrittlement in structural materials. Acta Mater 2019;165:734–50. https://doi.org/10.1016/j.actamat.2018.12.014.

[19] Robertson IM, Sofronis P, Nagao A, Martin ML, Wang S, Gross DW, et al. Hydrogen embrittlement understood. Metall Mater Trans A Phys Metall Mater Sci 2015;46:2323–41. https://doi.org/10.1007/s11661-015-2836-1.

[20] Li X, Ma X, Zhang J, Akiyama E, Wang Y, Song X. Review of hydrogen embrittlement in metals: hydrogen diffusion, hydrogen characterization, hydrogen embrittlement mechanism and prevention. Acta Metall Sin (English Lett 2020;33:759–73. https://doi.org/10.1007/s40195-020-01039-7.

[21] Pfeil LB. A PRSL. The effect of occluded hydrogen on the tensile strength of iron. Proc R Soc Lond - Ser A Contain Pap a Math Phys Character 1926;112:182–95. https://doi.org/10.1098/rspa.1926.0103.

[22] Oriani RA. A mechanistic theory of hydrogen embrittlement of steels. Berichte Der Bunsengesellschaft Für Phys Chemie 1972;76:848–57. https://doi.org/10.1002/BBPC.19720760864.

[23] Djukic MB, Bakic GM, Sijacki Zeravcic V, Sedmak A, Rajicic B. The synergistic action and interplay of hydrogen embrittlement mechanisms in steels and iron: localized plasticity and decohesion. Eng Fract Mech 2019;216:106528. https://doi.org/10.1016/j.engfracmech.2019.106528.

[24] Nagao A, Dadfarnia M, Somerday BP, Sofronis P, Ritchie RO. Hydrogen-enhanced-plasticity mediated decohesion for hydrogen-induced intergranular and “quasi-cleavage” fracture of lath martensitic steels. J Mech Phys Solid 2018;112:403–30. https://doi.org/10.1016/j.jmps.2017.12.016.

[25] Novak P, Yuan R, Somerday BP, Sofronis P, Ritchie RO. A statistical, physical-based, micro-mechanical model of hydrogen-induced intergranular fracture in steel. J Mech Phys Solid 2010;58:206–26. https://doi.org/10.1016/j.jmps.2009.10.005.

[26] Benedetti I, Gulizzi V, Milazzo A. Grain-boundary modelling of hydrogen assisted intergranular stress corrosion cracking. Mech Mater 2018;117:137–51. https://doi.org/10.1016/j.mechmat.2017.11.001.

[27] Dutton R, Nuttall K, Puls MP, Simpson LA. Mechanisms OF hydrogen induced delayed cracking IN hydride forming materials. OR Trans 1977;8(A):1553–62. https://doi.org/10.1007/BF02644858.

[28] Beachem CD. A new model for hydrogen-assisted cracking (hydrogen “embrittlement”). Metall Trans 1972;3:441–55. https://doi.org/10.1007/BF02642048.

[29] Birnbaum HK, Sofronis P. Hydrogen-enhanced localized plasticity-a mechanism for hydrogen-related fracture. Mater Sci Eng, A 1994;176:191–202. https://doi.org/10.1016/0921-5093(94)90975-X.

[30] Ferreira PJ, Robertson IM, Birnbaum HK. Hydrogen effects on the interaction between dislocations. Acta Mater 1998;46:1749–57. https://doi.org/10.1016/S1359-6454(97)00349-2.

[31] Robertson IM, Birnbaum HK. An HVEM study of hydrogen effects on the deformation and fracture of nickel. Acta Metall 1986;34:353–66. https://doi.org/10.1016/0001-6160(86)90071-4.

[32] Song J, Curtin WA. Atomic mechanism and prediction of hydrogen embrittlement in iron. Nat Mater 2013;12:145–51. https://doi.org/10.1038/nmat3479.

[33] Song J, Curtin WA. A nanoscale mechanism of hydrogen embrittlement in metals. Acta Mater 2011;59:1557–69. https://doi.org/10.1016/J.ACTAMAT.2010.11.019.

[34] Morita S, Kitagawa K, Miyata Y. Hydration structure of a nafion membrane in a polymer electrolyte fuel cell. In: 46th AIAA/ASME/SAE/ASEE jt. Propuls. Conf. & exhib. Reston, Virigina: American Institute of Aeronautics and Astronautics; 2010. 10.2514/6.2010-6922.

[35] Matsumoto R, Taketomi S, Matsumoto S, Miyazaki N. Atomistic simulations of hydrogen embrittlement. Int J Hydrogen Energy 2009;34:9576–84. https://doi.org/10.1016/j.ijhydene.2009.09.052.

[36] Xing X, Deng G, Zhang H, Cui G, Liu J, Li Z, et al. Molecular dynamics studies of hydrogen effect on intergranular fracture in α-iron. Materials 2020;13:4949. https://doi.org/10.3390/ma13214949.

[37] Jung SP, Kwon Y, Lee CS, Lee BJ. Influence of hydrogen on the grain boundary crack propagation in bcc iron: a molecular dynamics simulation. Comput Mater Sci 2018;149:424–34. https://doi.org/10.1016/j.commatsci.2018.03.053.

[38] Zhou XY, Yang XS, Zhu JH, Xing F. Atomistic simulation study of the grain-size effect on hydrogen embrittlement of nanograined Fe. Int J Hydrogen Energy 2020;45:3294–306. https://doi.org/10.1016/j.ijhydene.2019.11.131.

[39] Zhu Y, Li Z, Huang M. Solute hydrogen effects on plastic deformation mechanisms of A-Fe with twist grain boundary. Int J Hydrogen Energy 2018;43:10481–95. https://doi.org/10.1016/j.ijhydene.2018.04.133.

[40] Song J, Curtin WA. Mechanisms of hydrogen-enhanced localized plasticity: an atomistic study using α-Fe as a model system. Acta Mater 2014;68:61–9. https://doi.org/10.1016/j.actamat.2014.01.008.

[41] Zhu Y, Li Z, Huang M, Fan H. Study on interactions of an edge dislocation with vacancy-H complex by atomistic modelling. Int J Plast 2017;92:31–44. https://doi.org/10.1016/j.ijplas.2017.03.003.

[42] Katzarov IH, Pashov DL, Paxton AT. Hydrogen embrittlement I. Analysis of hydrogen-enhanced localized plasticity: effect of hydrogen on the velocity of screw dislocations in α -Fe. Phys Rev Mater 2017;1:1–11. https://doi.org/10.1103/PhysRevMaterials.1.033602.

[43] Plimpton S. Fast parallel algorithms for short-range molecular dynamics. J Comput Phys 1995;117:1–19. https://doi.org/10.1006/jcph.1995.1039.

[44] Franciosi P. Glide mechanisms in b.c.c. crystals: an investigation of the case of α-iron through multislip and latent hardening tests. Acta Metall 1983;31:1331–42. https://doi.org/10.1016/0001-6160(83)90004-4.

[45] Spitzig WA, Keh AS. The effect of orientation and temperature on the plastic flow properties of iron single crystals. Acta Metall 1970;18:611–22. https://doi.org/10.1016/0001-6160(70)90090-8.

[46] Scheiber D, Pippan R, Puschnig P, Romaner L. Ab initio calculations of grain boundaries in bcc metals. Model Simulat Mater Sci Eng 2016;24:35013. https://doi.org/10.1088/0965-0393/24/3/035013.

[47] Ramasubramaniam A, Itakura M, Carter EA. Interatomic potentials for hydrogen in α -iron based on density functional theory. Phys Rev B Condens Matter 2009;79:1–13. https://doi.org/10.1103/PhysRevB.79.174101.

[48] Zhou XY, Zhu JH, Wu HH. Molecular dynamics studies of the grain-size dependent hydrogen diffusion coefficient of nanograined Fe. Int J Hydrogen Energy 2021;46:5842–51. https://doi.org/10.1016/j.ijhydene.2020.11.131.

[49] Wang Z, Shi X, Yang XS, He W, Shi SQ, Ma X. Atomistic simulation of the effect of the dissolution and adsorption of hydrogen atoms on the fracture of α-Fe single crystal under tensile load. Int J Hydrogen Energy 2021;46:1347–61. https://doi.org/10.1016/j.ijhydene.2020.09.216.

[50] Ramunni VP, Pascuet MI, Castin N, Rivas AMF. The influence of grain size on the hydrogen diffusion in bcc Fe. Comput Mater Sci 2021;188:110146. https://doi.org/10.1016/j.commatsci.2020.110146.

[51] Daw MS, Baskes MI. Semiempirical, quantum mechanical calculation of hydrogen embrittlement in metals. Phys Rev Lett 1983;50:1285–8. https://doi.org/10.1103/PhysRevLett.50.1285.

[52] Stukowski A. Visualization and analysis of atomistic simulation data with OVITO–the Open Visualization Tool. Model Simulat Mater Sci Eng 2010;18:015012. https://doi.org/10.1088/0965-0393/18/1/015012.

[53] Stukowski A, Bulatov VV, Arsenlis A. Automated identification and indexing of dislocations in crystal interfaces. Model Simulat Mater Sci Eng 2012;20:085007. https://doi.org/10.1088/0965-0393/20/8/085007.

[54] Zhou M. A new look at the atomic level virial stress: on continuum-molecular system equivalence. Proc R Soc A Math Phys Eng Sci 2003;459:2347–92. https://doi.org/10.1098/rspa.2003.1127.

[55] Peierls R. The size of a dislocation. Proc Phys Soc 1940;52:34–7. https://doi.org/10.1088/0959-5309/52/1/305.

[56] Hirth J. Theory of dislocations john price hirth [and] jens lothe. 1967.

[57] Monnet G, Terentyev D. Structure and mobility of the frac(1, 2) < 1 1 1 > {1 1 2} edge dislocation in BCC iron studied by molecular dynamics. Acta Mater 2009;57:1416–26. https://doi.org/10.1016/j.actamat.2008.11.030.

[58] Queyreau S, Marian J, Gilbert MR, Wirth BD. Edge dislocation mobilities in bcc Fe obtained by molecular dynamics. Phys Rev B Condens Matter 2011;84:1–7. https://doi.org/10.1103/PhysRevB.84.064106.

[59] Po G, Cui Y, Rivera D, Cereceda D, Swinburne TD, Marian J, et al. A phenomenological dislocation mobility law for bcc metals. Acta Mater 2016;119:123–35. https://doi.org/10.1016/j.actamat.2016.08.016.

[60] Brailsford AD. Anharmonicity contributions to dislocation drag. J Appl Phys 1972;43:1380–93. https://doi.org/10.1063/1.1661329.

[61] Robertson IM, Martin ML, Fenske JA. Influence of hydrogen on the behavior of dislocations. Gaseous hydrog. Embrittlement mater. Energy technol. Mech. Model. Futur. Dev.. Elsevier Inc.; 2012. p. 166–206. https://doi.org/10.1533/9780857095374.1.166.

[62] Chapter 4 frictional forces in metals. Pergamon mater. Ser. vol. 8. Elsevier Ltd; 2003. p. 85–123. https://doi.org/10.1016/S1470-1804(03)80034-2.

[63] Xie W, Liu X, Chen W, Zhang H. Hydrogen hardening effect in heavily deformed single crystal α-Fe. Comput Mater Sci 2011;50:3397–402. https://doi.org/10.1016/j.commatsci.2011.06.036.

[64] Zhao Y, Seok MY, Choi IC, Lee YH, Park SJ, Ramamurty U, et al. The role of hydrogen in hardening/softening steel: influence of the charging process. Scripta Mater 2015;107:46–9. https://doi.org/10.1016/j.scriptamat.2015.05.017.

[65] Taketomi S, Matsumoto R, Hagihara S. Molecular statics simulation of the effect of hydrogen concentration on {112} <111> edge dislocation mobility in alpha iron. ISIJ Int 2017;57:2058–64. https://doi.org/10.2355/isijinternational.ISIJINT-2017-172.

[66] Matsui H, Kimura H, Moriya S. The effect of hydrogen on the mechanical properties of high purity iron I. Softening and hardening of high purity iron by hydrogen charging during tensile deformation. Mater Sci Eng 1979;40:207–16. https://doi.org/10.1016/0025-5416(79)90191-5.

[67] Taketomi S, Matsumoto R, Miyazaki N. Atomistic study of the effect of hydrogen on dislocation emission from a mode II crack tip in alpha iron. Int J Mech Sci 2010;52:334–8. https://doi.org/10.1016/j.ijmecsci.2009.09.042.

[68] Zhou G, Zhou F, Zhao X, Zhang W, Chen N, Wan F, et al. Molecular dynamics simulation of hydrogen enhancing dislocation emission. Sci China, Ser E Technol Sci 1998;41:176–81. https://doi.org/10.1007/bf02919680.

[69] Li J, Lu C, Pei L, Zhang C, Wang R. Hydrogen-modified interaction between lattice dislocations and grain boundaries by atomistic modelling. Int J Hydrogen Energy 2020;45:9174–87. https://doi.org/10.1016/j.ijhydene.2020.01.103.

[70] Adlakha I, Solanki KN. Critical assessment of hydrogen effects on the slip transmission across grain boundaries in α-Fe. Proc R Soc A Math Phys Eng Sci 2016;472. https://doi.org/10.1098/rspa.2015.0617.

[71] Zhou XY, Zhu JH, Wu HH, Yang XS, Wang S, Mao X. Unveiling the role of hydrogen on the creep behaviors of nanograined α-Fe via molecular dynamics simulations. Int J Hydrogen Energy 2021;46:9613–29. https://doi.org/10.1016/j.ijhydene.2020.12.115.